4-8-1998

Quadratic Electro-Optic Effects in Bacteriorhodopsin: Measurement of γ(-ω;0,0,ω) in Dried Gelatin Thin Films

Mikio Yamazaki
Syracuse University

Jerry Goodisman
Syracuse University

Robert R. Birge
Syracuse University

Quadratic electro-optic effects in bacteriorhodopsin: Measurement of γ(−ω;0,0,ω) in dried gelatin thin films

Mikio Yamazaki, Jerry Goodisman, and Robert R. Birge

Citation: J. Chem. Phys. **108**, 5876 (1998); doi: 10.1063/1.475998
View online: http://dx.doi.org/10.1063/1.475998
View Table of Contents: http://jcp.aip.org/resource/1/JCPSA6/v108/i14
Published by the American Institute of Physics.

Quadratic electro-optic effects in bacteriorhodopsin: Measurement of $\gamma(-\omega;0,0,\omega)$ in dried gelatin thin films

Mikio Yamazaki,[a] Jerry Goodisman, and Robert R. Birge[b]
Department of Chemistry and W. M. Keck Center for Molecular Electronics, Syracuse University, Syracuse, New York 13244-4100

(Received 13 November 1997; accepted 7 January 1998)

Quadratic electro-optic effects (dc or low frequency Kerr effect) of bacteriorhodopsin dispersed in dried gelatin thin films are examined in the near resonance region at three wavelengths: 633, 647, and 676 nm. The films show relatively large quadratic electro-optic effects compared to other molecular dispersed systems. The purple membrane is fixed within the polymerized gelatin matrix, and we show that the electronic contribution to γ dominates over possible orientational contributions. At 676 nm, the quadratic electro-optic coefficient $s_{1133}(-\omega;0,0,\omega)$ is 6.7×10^{-20} m^2/V^2 and the third order nonlinear susceptibility $\chi^{(3)}_{1133}(-\omega;0,0,\omega)$ is 7.0×10^{-13} cm^4 $statCoulomb^{-2}$, with both values obtained for a protein concentration of 6.9×10^{18} cm^{-3}. The orientationally averaged second molecular hyperpolarizability $\langle\gamma(-\omega;0,0,\omega)\rangle$ determined from the quadratic electro-optic coefficients at 676 nm assuming an Onsager ellipsoidal local field factor is $(10.8\pm5.1)\times10^{-32}$ cm^7 $statCoulomb^{-2}$ $[(1.34\pm0.63)\times10^{-56}$ F^3 m^4 $C^{-2}]$. The $\langle\gamma(-\omega;0,0,\omega)\rangle$ value increases roughly tenfold when the probe wavelength is decreased to 633 nm. The behavior of $\gamma(-\omega;0,0,\omega)$, when fit to a two-state model, predicts that $\gamma(-\omega;0,0,\omega)$ is strongly enhanced via type III processes. Thus, the magnitude of $\gamma(-\omega;0,0,\omega)$ is dominated by a term $(\Delta\mu_{10}^2\times\mu_{10}^2)/(\omega_{10}-\omega)^3$, where $\Delta\mu_{10}$ is the change in dipole moment, μ_{10} is the transition moment, and ω_{10} is the transition energy of the lowest-lying allowed $^1B_u^{*+}$-like π,π^* state. We calculate that $\Delta\mu_{10}$ is 12.8 ± 1.2 D, in good agreement with previous Stark and two-photon experimental values. Time-dependent Hartree–Fock methods based on the MNDO Hamiltonian yield reasonable agreement with experiment, underestimating $\gamma(-\omega;0,0,\omega)$ by factors of only 2–4, with the error increasing as the frequency approaches resonance. © *1998 American Institute of Physics.* [S0021-9606(98)01114-3]

I. INTRODUCTION

Bacteriorhodopsin (BR, M.W.≈26 000) is the light transducing protein found in the purple membrane formed in the cell wall of the bacterium, *Halobacterium salinarium*.[1–11] The physiological function of this protein is to produce energy for converting ADP to ATP by pumping protons from the cytoplasmic to the extracellular side of the cell wall. The resulting pH gradient across the cell wall generates a proton motive force for synthesizing ATP. The proton pumping process is mediated by a complex photocycle which is illustrated in Fig. 1. When bacteriorhodopsin first absorbs light, it converts from the dark-adapted form to a light-adapted form (bR), which contains only an all-*trans* protonated Schiff base chromophore. Unless specified otherwise, all of our experiments and all similar studies in the literature were carried out on the light-adapted form.

Bacteriorhodopsin is known to exhibit large optical nonlinearities, due in part to the large difference between the dipole moment in the ground state and that in its lowest-lying, strongly allowed excited state.[12–19] The first measurement of β by Huang *et al.* gave a value of 2500×10^{-30} cm^5 $statcoulomb^{-1}$, approximately ten times larger than other organic chromophores of comparable conjugation length.[19] Subsequent studies yielded a comparable value of $2250\pm240\times10^{-30}$ cm^5 $statcoulomb^{-1}$ based on an analysis of the two-photon double resonance spectrum.[12] Analysis of the two-photon data also indicate that γ should be relatively large, due in part to the large change in dipole moment upon excitation (type III enhancement).[15,20]

In this study, we report the direct observation of γ of bR dispersed in dried gelatin thin films in the near resonance region. Our experimental method is based on the technique proposed by Schildkraut for measuring linear electrooptic effects by using a reflection geometry.[21] In this experiment, gelatin films containing bR were formed on ITO covered glass substrates and Au electrodes were deposited on the surface of the gelatin films. A low frequency electric field is applied to the gelatin film to induce birefringence. Low intensity laser light is then directed onto the film through the ITO coated glass substrate. The laser light propagating inside the gelatin film is then reflected back by the surface of the Au electrode. The electromagnetic field associated with the laser light is modulated with a change in the phase difference between **s**- and **p**-polarized component caused via linear electro-optic effects and/or quadratic electrooptic effect (also referred to as dc or low frequency Kerr effects).

[a]Present address: Fuji Electric Corporate Research and Development, Ltd., 2-2-1 Nagasaka Yokosuka 240-0194, Japan.
[b]Author to whom correspondence should be addressed.

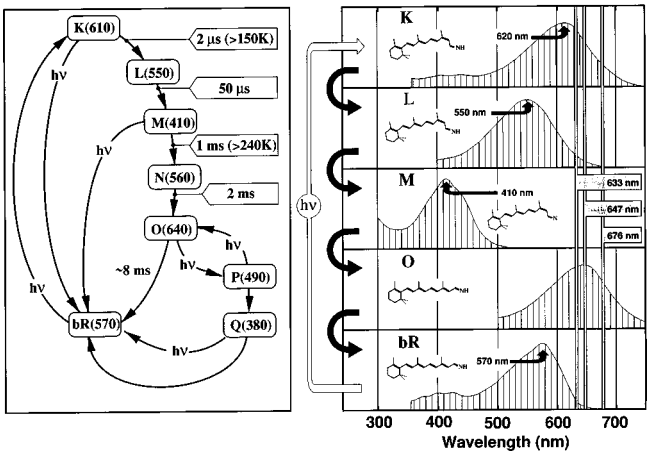

FIG. 1. Schematic diagram of the photocycle of light adapted bacteriorhodopsin (left) and absorption spectra of selected intermediates (right). Bold letters denote intermediates in the photocycle, and approximate absorption maxima of the intermediates are shown in nm. The abbreviation **bR** denotes the ground state of light adapted bacteriorhodopsin. Arrows without the label ''$h\nu$'' indicate thermal decay. The three wavelengths used in our electro-optical measurements are indicated with vertical bars at right.

Gelatin has been known to have a cross-linked, collagen-like structure with hydrogen bonds. When purple membrane is immersed in the gelatin matrix, the purple membrane is considered to be spatially fixed. The interaction between the host molecule and the gelatin matrix via the hydrogen bonds is expected to play a role in preventing induction of molecular orientation under strong modulation field. For example, Ho *et al.* investigated linear electro-optic effects of *p*-nitrophenol in a gelatin matrix and observed that the gelatin matrix maintained poling stability.[22] Thus, we conclude that orientational contributions to the measured electro-optic effect can be ignored. Our experimental results provide support for this conclusion. By analyzing the wavelength dependence of γ, we gain insight into the electronic origin of the large second order hyperpolarizability of bacteriorhodopsin.

II. EXPERIMENT

A. Sample preparation

Purple membrane was isolated from the strain S9-P of *Halobacterium salinarium* by using the following procedure. The bacterium was collected by spinning down the culture containing the bacterium in a Beckman JA-10 rotor at 5000 rpm (15 000 g) for 10–15 min, then resuspending in distilled water. The total volume of the suspension was approximately 500 mL. We then added 0.15 mg/mL of DNAse I type IV (Sigma D-5025) and 0.25 g of $MgSO_4$ to the suspension to digest the DNA contaminant. The suspension was left over night with gentle stirring at ambient temperature, and the cell debris was removed by spinning the sample down using a Beckman JA-17 rotor at 5000 rpm for 5 to 10 min.

The supernatant and purple membrane were saved and spun down in a 45 Ti rotor at 32 000 rpm (109 000 g) for 35 min at 4 °C. Pellets of purple membrane which formed at the bottom of the centrifuge tubes were washed via resuspension in de-ionized water, followed by centrifugation as described above. This procedure was repeated until the supernatant became clear. Brownish cell debris found in the pellet at bottom of centrifuge tubes was removed mechanically.

The gelatin thin films dispersed with the purple membrane were prepared as follows. Gelatin (gelatin type A from porcine skin [CAS# 9000-70-8], Sigma Chemical Co., used as received) was dissolved in deionized water by heating to 60–65 °C for 40 min in a round bottom flask equipped with a water condenser on a water bath. The concentration of gelatin was 10 w/w% in de-ionized water. After the gelatin was completely dissolved, the solution was filtered with a syringe filter (pore size 5 μm Micron Separations Inc.) while the solution was still hot. The suspension of bacteriorhodopsin in deionized water was spun down in the Beckman 45 Ti rotor (32 000 rpm, 109 000 g for 30 min) to yield a pellet of purple membrane. The pellet was resuspended in a minimal amount of deionized water. Then the suspension was sonicated for 30 min. The sonicator tip was directly immersed in the suspension for efficient sonication.

The gelatin solution and protein suspension were filtered with a syringe filter (AcetatePlus Membrane, pore size 5 μm, diameter 25 mm, Micron Separations Inc.), heated to 60 °C, and then mixed with gentle stirring for about 30 min while maintaining the temperature at 60 °C. The resulting mixture was coated onto an indium tin oxide (ITO) coated BK-7 glass substrate via the spin coating method. The thickness of the ITO coating was approximately 1000 Å yielding a resistivity of about 1 kΩ cm. Spin coating was carried out by pipetting 200–250 μL of the protein:gelatin mixture onto the preheated ITO coated substrate so that the mixture covered the surface as uniformly as was possible. The substrate was then transferred to the spin coating apparatus, and the thickness of the final film was controlled by adjusting the rotational speed of the spin coater. By using this procedure, film thicknesses ranging from 3 to 15 μm were achieved.

After the films had formed on the ITO covered glass substrates, they were dried in a closed container, in which the relative humidity was maintained at 80% to 85% and temperature was maintained at 25 °C for two days. The humidity was controlled by placing a beaker containing a saturated KCl solution inside the container.

The film thickness was measured by taking transmittance spectra from the visible to the near ir region. An interference pattern was found in the transmittance spectra when the surface quality of the films was high, and the films were of uniform thickness. All further optical studies were carried out only on those films which satisfied the above two criteria. The film thickness was determined from the interference pattern by using the following equation:

$$l = \frac{\Delta m}{2\sqrt{n^2 - \sin^2\theta}} \left(\frac{1}{1/\lambda_2 - 1/\lambda_1} \right), \tag{1}$$

where l is the film thickness, Δm is the number of peaks (or valleys) in the interference pattern, λ_1 is the longest wavelength in the interference pattern, λ_2 is the shortest wave length in the interference pattern, θ is the incident angle of a probe beam and n is the refractive index of the films (n

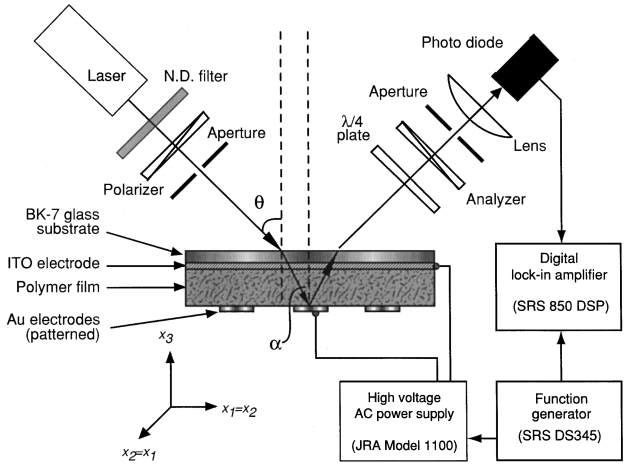

FIG. 2. The apparatus used to measure the nonlinear electrooptical properties of the protein thin films. The x_1, x_2, and x_3 axes were taken as a coordinate system fixed inside the film, where the x_3 axis is perpendicular to the film surface and x_1 and x_2 are parallel to the film surface. Also, θ denotes the incident angle of the laser and α denotes an effective propagation angle of the laser inside the film. The relative thickness of the glass substrate is unrealistically small for graphical convenience.

$=1.53$, see below). The transmittances were measured using a Shimadzu UV-3101 UV-Vis-NIR spectrometer with optical film thickness measurement software.

After the film thickness was confirmed, four to six round Au thin film electrodes were deposited directly onto the surface of the protein:gelatin film by using a dc sputtering process. Film thickness of the Au electrode was approximately 1000 Å and its diameter was 0.525 cm. Because the sputtering process removes moisture from the gelatin film, the gelatin film directly under the Au electrodes shrunk causing distortion of the film. To remove the distortion, the films were placed in the humidity and temperature controlled container again for at least five days. Prior to carrying out our optical measurements,the films were stored for two days at ambient temperature and about 65% relative humidity.

B. Electrooptic light modulation with quadratic electrooptic effects

Figure 2 shows the experimental setup for the electrooptic response measurement using the reflection technique. Radiation from a He–Ne laser (05LHP151 5 mW polarized laser head, Melles-Griot, Irvine CA) or a Krypton ion laser (Innova-301, 750 mW, Coherent Corp., Palo Alto CA) provided the probe irradiation. Light intensity was measured with a photodiode (Model 2001 optical receiver, New Focus, Mountainview, CA) and a digital multimeter (Keithley 179A TRMS), and all intensities were corrected by the response factors of the photodiode. Data were collected at three wavelengths: 632.8 nm (He–Ne), 647.1 nm (Kr ion) and 676.4 nm (Kr ion). These wavelengths correspond to the near absorption edge region of the ground state of the bacteriorhodopsin (Fig. 1).

Polarization of the incident light was adjusted to 45 degrees with respect to the plane of incidence with a glan-laser prism so that the electric field vector of the incident light yielded an equal amount of **s**- and **p**-polarized components. The reflected beam was passed through a zero order quarter wave plate followed by a second glan-laser prism,which was set to be cross-Nicol relative to the first prism. The quarter wave plate thus gives 90 degree phase biasing to the reflected beam. The rotation angle of the quarter wave plate was adjusted so that the maximum output power was obtained.

After the reflected beam was passed through the second aperture, it was focused to fill but not overflow the active area of the photodiode. The photodiode was carefully shielded with Cu mesh to eliminate signal due to the stray emf from the high voltage power supply and associated leads. The output signal from the photodiode was fed into a digital lock-in amplifier (SRS850 DSP, Stanford Research Systems, Sunnyvale, CA). A TTL reference signal at 500 Hz was provided to the lock-in amplifier using a synthesized function generator (DS345 Synthesized Function Generator, Stanford Research Systems). The function generator also provided a synchronized signal to the ac power supply (Model 1100 High voltage ac power supply, Joseph Rolfe Associates, Palo Alto Stanford, CA). The high voltage power supply was driven well below its rms capacity to avoid nonsinusoidal behavior and no bias was added to the signal to avoid creating a net orientational (poling) applied field.

C. Signal analysis

In the weak poling limit, the refractive index change associated with an external applied electric field can be written for ordinary and extraordinary rays as follows:

$$\Delta n_o = \tfrac{1}{2} n_o^3 (r_{113} E_3 + s_{1133} E_3 E_3), \tag{2a}$$

$$\Delta n_e = \tfrac{1}{2} n_e^3 (r_{333} E_3 + s_{3333} E_3 E_3), \tag{2b}$$

where r_{113} and r_{333} are the linear electrooptic coefficients measured along in-plane and film normal directions, respectively, and s_{1133} and s_{3333} are the quadratic electro-optic coefficients measured along the in-plane and film normal directions, respectively. The Schildkraut derived expression for the degree of the phase modulation in the reflection geometry is

$$\Gamma = \frac{4\pi}{\lambda} l \Delta\Delta n \frac{\sin^2 \alpha}{\cos \alpha}, \tag{3a}$$

$$\Delta\Delta n = \Delta n_e - \Delta n_o . \tag{3b}$$

Assuming Kleinman's symmetry holds ($r_{333}=3r_{113}$, $s_{3333}=3s_{1133}$) and $n_o \sim n_e \sim n$, Eq. (3a) becomes

$$\Gamma = \frac{4\pi l n^3}{\lambda} [r_{113} E_3 + s_{1133} E_3 E_3] \frac{\sin^2 \alpha}{\cos \alpha}. \tag{4}$$

When the modulation field can be represented as a simple ac field $[E_m = (V_m/l)\cos \Omega t]$, the relationship between the phase shift, Γ, and the modulated laser light intensity ratio, I_{ac}/I_{dc}, can be calculated as follows:[23,24]

$$\frac{I_{\rm ac}}{I_{\rm dc}} = 2\sin^2\left[\frac{1}{2}\left(\frac{\pi}{2}+\Gamma\right)\right]$$
$$\approx 1-\frac{\pi}{2}+\frac{8\pi}{\lambda}\frac{\sin^2\alpha}{\cos\alpha}\left[\Delta n_{\rm abs}l+\frac{n^3 s_{1133}V_m^2}{4l}\right.$$
$$\left.+\frac{n^3 r_{113}V_m}{2}\cos\Omega t+\frac{n^3 s_{1133}V_m^2}{4l}\cos 2\Omega t\right], \qquad (5)$$

where l is film thickness, V_m is applied voltage, I_{ac} is degree of modulation and $I_{\rm dc}$ is defined as the dc signal obtained by subtracting the dc level with the quarter wave plate with applying no modulation voltage from the dc level without the quarter wave plate with applying no modulation voltage. The dc signal thus corresponds to 50% transmittance, and the $\pi/2$ phase biasing has been added into Eq. (5). The phase biasing is achieved by placing the quarter wave ($\lambda/4$) plate into the optical path as shown in Fig. 2. The term $\Delta n_{\rm abs}$ arises from the absorption change of the medium and does not depend on the modulation field. The system is considered to be isotropic, and thus the term involving r_{113} is either not detectable or negligible compared to the term involving s_{1133}. Only the term depending on $\cos 2\Omega t$ is detected by the lock-in amplifier at the second harmonic frequency of the modulation field. The degree of modulation at the second harmonic frequency is defined as

$$\frac{I_{\rm ac}^{2\Omega}}{I_{\rm dc}} = \Delta\Gamma^{2\Omega}\cos 2\Omega t = \frac{2\pi n^3 s_{1133}V_m^2}{\lambda l}\frac{\sin^2\alpha}{\cos\alpha}\cos 2\Omega t, \qquad (6)$$

where $\Delta\Gamma^{2\Omega}$ is the amplitude of the phase shift modulation. The relation between the effective propagation angle, α, and the incident angle, θ, is given by Snell's law

$$\sin\theta = n\sin\alpha. \qquad (7)$$

Considering Eq. (7) and assuming that both the modulation field and the modulated light amplitude are measured as rms amplitudes, Eq. (6) reduces to

$$s_{3333}^{\rm expt} = \frac{3\lambda l}{2\sqrt{2}\pi(V_m^{\rm rms})^2}\frac{\sqrt{n^2-\sin^2\theta}}{n^2\sin^2\theta}\frac{I_{\rm ac}^{2\Omega,\rm expt}}{I_{\rm dc}}. \qquad (8)$$

III. RESULT AND DISCUSSION

A. Quadratic electrooptic effects observed in the gelatin films containing bR

Figure 3 shows a typical electrooptic response from bacteriorhodopsin dispersed in gelatin film obtained using 632.8 nm laser radiation. Signal amplitudes at the second harmonic frequency (1 kHz) were typically 2 to 3 orders of magnitude larger than those at the fundamental frequency (500 Hz). Signals at a fundamental frequency based on linear electro-optic effects were not detectable in most cases, because the protein samples are highly homogeneous and isotropic. However, the quadratic modulation voltage dependence of the signals at a second harmonic frequency were distinct and the raw signal intensity in rms voltage was on the order of 0.1–10 μV, levels readily observable by the digital lock-in amplifier. The modulated signal amplitudes normalized with the dc components were on the order of 10^{-4}–10^{-2}.

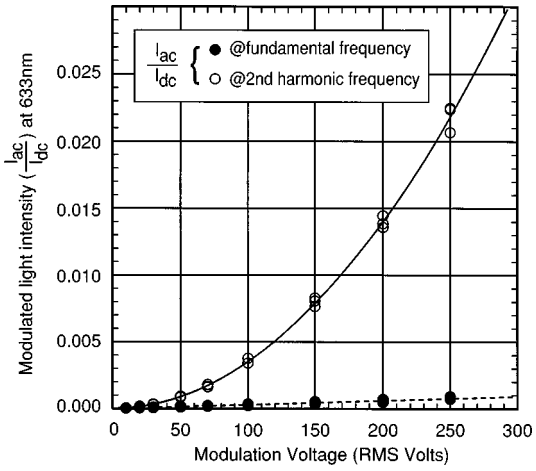

FIG. 3. Typical electrooptic response obtained from the bacteriorhodopsin dispersed in a dried gelatin thin film. The experiments were repeated three times to confirm reproducibility of the electrooptic response from the light adapted protein. Key experimental variables are as follows: modulation frequency, 500 Hz; film thickness, 15.3 μm; bR concentration, 6.9×10^{18} cm^{-3} and incident photon density, 2.4×10^{21} photons m^{-2} s^{-1}.

Three consecutive experiments were carried out for each sample at each wavelength (Fig. 3). Spectrophotometric studies were carried out to verify that the protein remained light-adapted during the experiment. Contributions to the quadratic electro-optic effects from gelatin itself were negligible. The normalized modulated light intensities were replotted against the quantity

$$\frac{(\text{rms amplitude of modulation voltage})^2}{\text{wavelength}\times\text{film thickness}}.$$

From the slopes of the curves obtained with this analysis, s_{1133} was calculated via Eq. (8). Figure 4 shows an example of the normalized intensity-normalized quadratic voltage plot

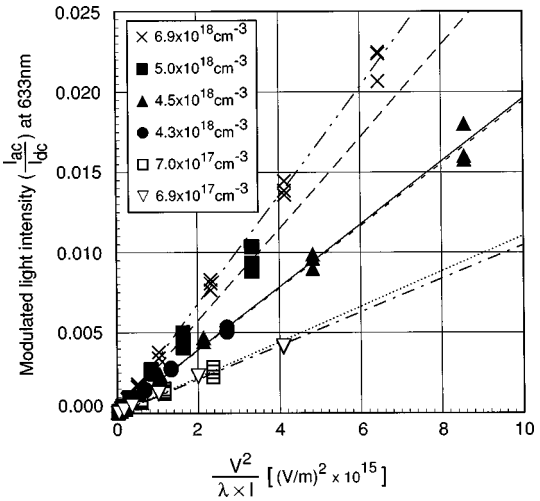

FIG. 4. Modulated light intensity-normalized quadratic voltage plots. These curves were measured with 633 nm incident light and 2.4×10^{21} m^{-2} s^{-1} of photon density for various protein concentrations. The data points were fitted with straight lines and slopes were obtained for the evaluation of s_{1133}. Similar data sets were acquired at 647.1 and 676.4 nm.

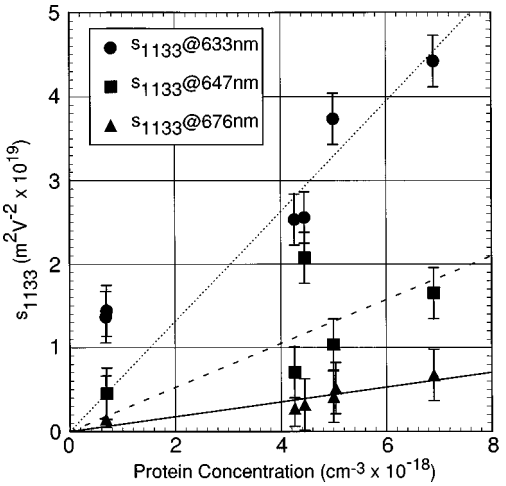

FIG. 5. Concentration dependence of the quadratic electro-optic effects of the gelatin films containing bacteriorhodopsin at several wavelengths in near resonance region. The quadratic electrooptic signals vary linearly with respect to the concentration of bacteriorhodopsin.

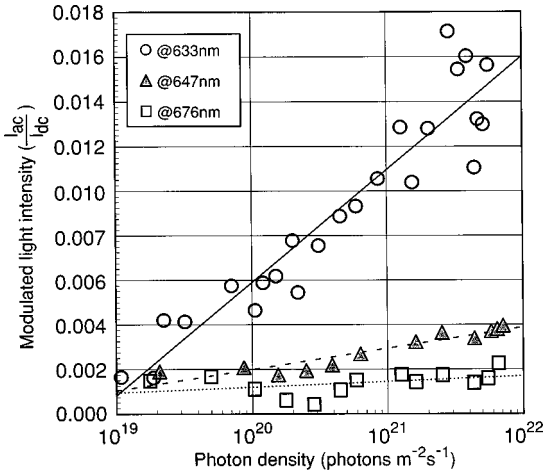

FIG. 6. Photon density dependence of the modulated light intensity detected at the second harmonic of the modulation frequency. The modulation voltage was fixed at 200 V rms, the film thickness was 15.3 μm, protein concentration was 6.9×10^{18} cm^{-3} and the modulation frequency was 500 Hz.

at 632.8 nm for a range in bacteriorhodopsin concentration from 6.9×10^{17} cm^{-3} to 6.9×10^{18} cm^{-3}. The curves shown in Fig. 4 were successfully fitted with straight lines with good correlation between the above two quantities. The same curve fitting procedures were used to analyze the data at 647.1 and 676.4 nm.

Figure 5 shows the bacteriorhodopsin concentration dependence of the quadratic electrooptic effects measured at several wavelengths. These data indicate that the quadratic electro-optic effects are approximately linear with respect to concentration of bacteriorhodopsin within the concentration range investigated here. This observation implies that the second molecular hyperpolarizability can be determined from the slopes of these curves. We can thus conclude with confidence that the protein, and not the gelatin matrix or other components along the light path, is responsible for the signal. It is thus possible to equate the measured value of $\chi^{(3)}$ to the molecular γ via the relation $\chi^{(3)}=NL\langle\gamma\rangle$, where N is the concentration of the protein and L is a local field correction.

Neither the linear nor the quadratic electrooptic effect is expected to be dependent on the incident light intensity, but dependent only on the amplitude of the modulated electric field. However, the modulated light intensities with the quadratic electrooptic effects detected at 633 nm are proportional to the logarithm of the photon density of the incident light while the signal levels measured at 647 and 676 nm are invariant to photon density as shown in Fig. 6.

One possible explanation for the anomalous signal enhancement at 633 nm is an increased population of the **O** state of bacteriorhodopsin, which has an absorption maximum at ~645 nm (see Fig. 1). Bacteriorhodopsin has a sufficient absorptivity at 633 nm to yield a small population of photocycling molecules within the irradiated volume element, and the **O** state has a relatively long lifetime (~4 ms). We conclude that the quadratic electro-optic effect is likely enhanced anomalously by **O** state interference. Regardless of the origin of the effect, we removed the interference by extrapolating our data back to low light levels where such interference was minimal.

B. Calculation of γ from s

The third-order nonlinear susceptibility is related to the quadratic electrooptic coefficient by the following relationship:

$$\chi^{(3)}_{1133}(-\omega;0,0,\omega)=\frac{n^4}{12\pi}\,s_{1133}(-\omega;0,0,\omega)\quad\text{(cgs-esu)}. \tag{9}$$

A relation between the macroscopic third order nonlinear susceptibility of the films and the second molecular hyperpolarizability of the protein can be derived by taking local field factors into account. However, the choice of a local field factor is not obvious, because we are dealing with a chromophore imbedded inside a complex binding site (see Fig. 7).[9,25] For this reason, we will investigate here a variety of local field factors. The local field factor introduced by Onsager has been used extensively for studies of nonlinear optical properties of organic molecules (Appendix A). The Onsager's local field factor was derived assuming that the molecule is a dipole placed in a virtual spherical cavity in a continuous dielectric matrix and the local field is a sum of the field inside the cavity and the reaction field resulting from an interaction between the dipole moment of a molecule in the cavity and a polarization induced in surrounding matter by an external field. However, the retinal chromophore considered here is a rod shaped polyene. Hence, an ellipsoidal cavity is considered to be more suitable in this case (Fig. 7).[26] The expressions of the local field factors for the ellipsoidal cavity at a static field $f^{(0)}_{\text{ellipse}}$ and at an optical frequency $f^{(\omega)}_{\text{ellipse}}$ are given in (A6) and (A7) in Appendix A, respectively. Also, the expressions of the local field factors for the spherical cavity at a static field $f^{(0)}_{\text{sphere}}$ and at an optical frequency $f^{(\omega)}_{\text{sphere}}$ are given in (A8) and (A9) in Appendix A, respectively. For example, $f^{(0)}_{\text{ellipse}}$ is given as follows:

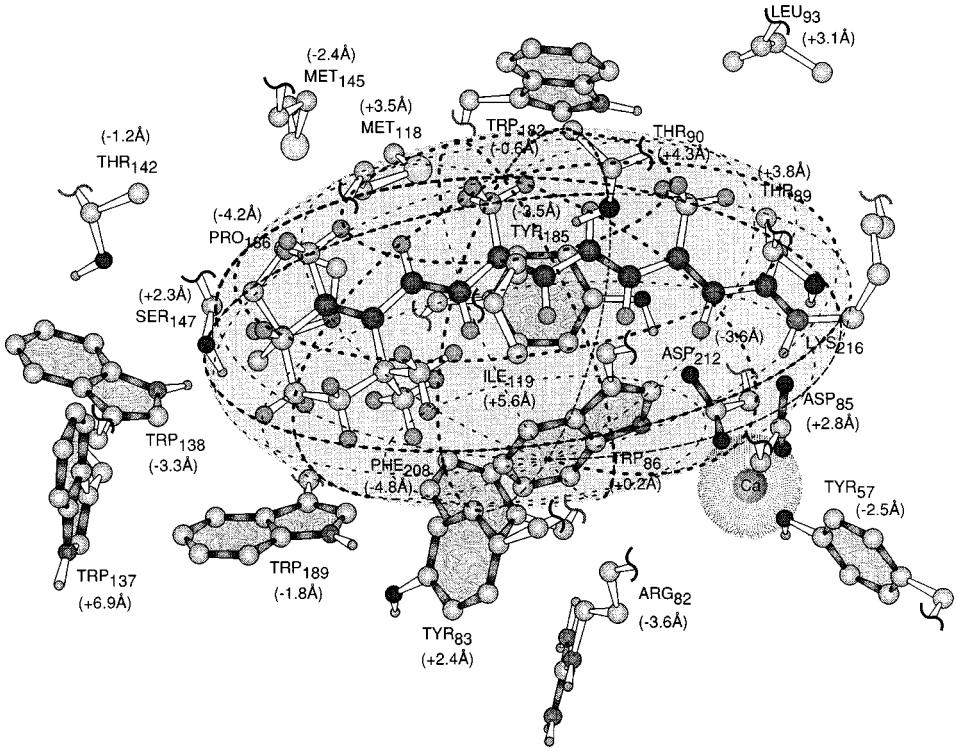

FIG. 7. A view of the chromophore binding site of light-adapted bacteriorhodopsin based on the model proposed by Henderson and co-workers obtained from electron cryomicroscopy diffraction studies (Ref. 9). The chromophore cavity used in the calculation of the Lorentz and Onsager elliptical local field calculations is superimposed. The numbers shown in parentheses give the center of mass displacements above (positive, out of the paper) and below (negative, into the paper) the chromophore polyene chain (in the plane of the paper). The putative position of calcium(II) is based on two-photon studies (Ref. 25).

$$f_{\text{ellipse}}^{(0)}=\frac{\epsilon_2(0)\{1+(\epsilon_1(\omega)-1)A_a\}}{\epsilon_2(0)+(\epsilon_1(\omega)-\epsilon_2(0))A_a}. \tag{A6}$$

An alternative, but widely accepted, approximation to the local field correction was developed by Lorentz. In the Lorentz's approximation, the reaction field is not taken into account. For comparison, the Lorentz-type local field factors for ellipsoidal and spherical cavities were also considered as the local field correction. The local field factors derived using the Lorentz approximation are given in (A14) and (A15) in Appendix A. For example, $f_{\text{sphere}}^{(\omega)}$ is given as follows:

$$f_{\text{sphere}}^{(\omega)}=\frac{\epsilon_2(\omega)+2}{3}. \tag{A15}$$

The permittivity of gelatin measured at 1 kHz ($\epsilon_2(0)=2.07$) was used as the static field permittivity of the polymer matrix. The refractive indices of the protein and the gelatin matrix at optical frequencies were taken from Song *et al.*[27] and were used for the calculation of the permittivities assuming $\epsilon_1(\omega)\cong n^2=(1.53)^2$ for bacteriorhodopsin and $\epsilon_2(\omega)\cong n^2=(1.54)^2$ for gelatin. The refractive index of opsin (the protein without the chromophore) was assumed to be equal to that of the gelatin matrix based on the experimental result for the effective dielectric constant of the protein in the **M** state ($\epsilon_2(0)=2.2$) obtained by Dioumaev *et al.*[28] The resulting local field factors are tabulated in Table I.

The molecular hyperpolarizability, γ, can now be related to the third order nonlinear susceptibility, $\chi^{(3)}$, by using the following relationship:

$$\chi_{ijkl}^{(3)}(-\omega;0,0,\omega)=Nf^{(0)}f^{(0)}f^{(\omega)}f^{(\omega)}\langle\gamma(-\omega;0,0,\omega)\rangle_{ijkl}, \tag{10}$$

where $\langle\gamma(-\omega;0,0,\omega)\rangle$ is an orientational average of γ over the molecular coordinates and N is concentration of the guest molecule. The subscripts i, j, k, and l denote film coordinates and $\chi_{ijkl}^{(3)}(-\omega;0,0,\omega)$ is a tensor component of $\chi^{(3)}$. The calculation of $\langle\gamma(-\omega;0,0,\omega)\rangle$ is discussed in Appendix B. If the films are isotropic, $\langle\gamma(-\omega;0,0,\omega)\rangle_{3333}$ is also an average value over the film coordinates, and the average value of γ over the film coordinate is given by

$$\langle\gamma\rangle\equiv\langle\gamma\rangle_{3333}=3\langle\gamma\rangle_{1133}. \tag{11}$$

TABLE I. Local field factors.[a]

Onsager-type local field factor				Lorentz-type local field factor			
$f_{\text{ellipse}}^{(0)}$	$f_{\text{ellipse}}^{(\omega)}$	$f_{\text{sphere}}^{(0)}$	$f_{\text{sphere}}^{(\omega)}$	$f_{\text{ellipse}}^{(0)}$	$f_{\text{ellipse}}^{(\omega)}$	$f_{\text{sphere}}^{(0)}$	$f_{\text{sphere}}^{(\omega)}$
1.28	1.33	1.39	1.45	1.26	1.33	1.36	1.46

[a]$n=1.53$ for bacteriorhodopsin, $n=1.54$ for gelatin matrix (from Ref. 27), $\epsilon=2.07$ for gelatin matrix at 1 kHz, $A_a=0.243$ (see discussion in Refs. 26, 31, 33).

TABLE II. Induced orientation effect for the quadratic electrooptic effect found in a gelatin film containing bacteriorhodopsin.

Concentration/cm^{-3}	$s_{1133}^{\text{expt.}}$/m^2 V^{-2}	s_{1133}^{sor}/m^2 V^{-2}	s_{1133}^{or}/m^2 V^{-2}
6.9×10^{18}	6.7×10^{-20}	8.7×10^{-26}	-3.2×10^{-27}

Thus, $\langle\gamma(-\omega;0,0,\omega)\rangle$ can be calculated from $\chi_{1133}^{(3)}(-\omega;0,0,\omega)$ by using Eqs. (10) and (11). The results are presented in Table IV. We consider the values for the Onsager elliptical local field factors to be the most experimentally relevant. The difference between the Onsager and Lorentz elliptical values, are, however much smaller than the experimental error. It would seem clear from an examination of Fig. 7 that an elliptical cavity is much more appropriate than a spherical cavity approximation.

C. Analysis with the two-state model

Kuzyk *et al.* have derived expressions for the second order induced orientational effects s_{1133}^{sor} and the orientational effect s_{1133}^{or} as follows:[29]

$$s_{1133}^{\text{sor}}=\frac{4\pi}{9\times10^8}\frac{N\beta_{zzz}^{*}\mu^{*}}{35k_\theta n^4}(14-50A_2+36A_4), \tag{12a}$$

$$s_{1133}^{\text{or}}=-\frac{1}{9\times10^8}\frac{16}{105}\pi N\alpha^{*}(-\Omega;\Omega)\frac{\alpha^{*}(-\omega;\omega)}{k_\theta n^4}\times(7+5A_2-12A_4). \tag{12b}$$

In these formulas, quantities with * denote local field corrected quantities and A_2 and A_4 are orientational order parameters. The factors A_2 and A_4 are zero for an isotropic system, k_θ is a microscopic elastic modulus constant in dyn cm, and k_θ is defined as a force constant of the restoring force F acting on the chromophore upon applying an electric field

$$F=\frac{k_\theta}{2}(\theta-\theta_0)^2. \tag{13}$$

In (13), $\theta-\theta_0$ is an angle variation between the direction of the applied electric field and the static dipole moment of the chromophore before and after applying the electric field. Alternatively, k_θ can also be estimated by multiplying the molecular volume of all-*trans* retinal, V, by the bulk modulus of the gelatin polymer, K, assuming that the purple membrane patches are strongly interacting with the gelatin matrix. For the present study, we use an ellipsoidal cavity volume instead of the molecular volume (see discussion below). Equations (12) and (13) were evaluated assuming $A_2=A_4=0$ (isotropic case) based on a bacteriorhodopsin concentration of 6.9×10^{18} cm^{-3}. The results are tabulated in Table II. All quantities not evaluated by us are available from the literature[30–33] and all relevant parameters are tabulated in Table III. Subtraction of s_{1133}^{sor} and s_{1133}^{or} from the experimentally measured value of s_{1133} should give a pure electronic contribution to the quadratic electrooptic effect. The total orientational correction for s_{1133} is consequently 8.5×10^{-26} m^2/V^2, which is negligible compared to the experimental result of s_{1133} obtained for this sample, 6.7×10^{-20} m^2/V^2. Therefore, the orientational contribution is negligible, and will be ignored in subsequent analyses.

Our experimental values of γ as a function of energy can be fit with good precision by using a very simple two variable nonlinear equation: $A/(\omega_B-\omega)^3$, where ω is the photon frequency and A and ω_B are the two variables. For reasons that will be clear from the subsequent discussion, this behavior is an indication that a single excited electronic state dominates the resonant enhancement of γ. This permits the use of a simple two level model of the process

$$\gamma_{i'i'i'i'}(-\omega_\sigma;\omega_1,\omega_2,\omega_3)=4K(-\omega_\sigma;\omega_1,\omega_2,\omega_3)(\hbar)^{-3}I_{-\sigma,1,2,3}\times\left[\frac{|\langle g|\mu_{i'}|n\rangle|^2\overline{\langle|n|\mu_{i'}|n\rangle|^2}}{(\omega_0-\omega_\sigma)(\omega_0-\omega_1-\omega_2)(\omega_0-\omega_1)}-\frac{|\langle g|\mu_{i'}|n\rangle|^4}{(\omega_0-\omega_\sigma)(\omega_0-\omega_1)(\omega_0+\omega_2)}\right], \tag{14}$$

where $\omega_0=\omega_{ng}$ corresponds to a transition frequency from a ground state to an excited state of interest, I denotes the average of all terms generated by permuting ω_σ, ω_1, ω_2, and ω_3 and K is a numerical factor that depends on the presence of zero frequencies and repeated frequencies in the set ω_σ, ω_1, ω_2, and ω_3. In addition, $\mu_{i'}$ is a ground state dipole moment of the chromophore along i' direction in the molecular coordinate, and $|n\rangle$ and $|g\rangle$ denote state vectors

TABLE III. Values used to calculate s^{sor},s^{or}.

$\alpha(-\Omega;\Omega)$/cm^{3a}	$\alpha(-\omega;\omega)$/cm^3	$\beta(-2\omega;\omega,\omega)$/esu[b]	μ/esu[a]	$f^{(0)}$	$f^{(\omega)}$
5.4×10^{-23}	3.0×10^{-23}	2.5×10^{-27}	5.3×10^{-18}	1.26	1.33

Bulk modulus K/dyn cm^{-2c}	Cavity volume V/cm^{3d}	Density N/cm^{-3}
1.71×10^{13}	4.02×10^{-22}	6.9×10^{18}

[a]This value was obtained for all-*trans*-retinal dissolved in hexane or cyclohexane based on electric field and refractive index measurements (Refs. 30, 31).
[b]This value was measured for bacteriorhodopsin dispersed in poly (vinyl alcohol) with second harmonic generation using a 1064 nm fundamental wavelength (Ref. 19).
[c]This value was measured as a Young's modulus at 20 °C and 65% relative humidity (Ref. 32). A rate of loading for the tensile strength testing was 25 kg cm^{-2} s^{-1}.
[d]From Refs. 26, 31.

for a nth state and a ground state of the chromophore, respectively. Equation (14) is a reduced expression of Eq. (B6) given in Appendix B.

Because the barred matrix element in Eq. (14) is defined as

$$\overline{\langle n|\mu_{i',j',k' \text{ or } l'}|n\rangle} \equiv \langle n|\mu_{i',j',k' \text{ or } l'}|n\rangle - \langle g|\mu_{i',j',k' \text{ or } l'}|g\rangle, \tag{15}$$

this term represents the dipole moment difference $\Delta\mu_{gn}$ between the ground state and the excited state. Also, $\langle g|\mu_{i',j',k' \text{ or } l'}|n\rangle$ is the transition moment associated with the $g \rightarrow n$ transition, and is thus proportional to the oscillator strength of the chromophore. Equation (14) can now be reduced to the simple form

$$\gamma_{10}(-\omega;0,0,\omega) \approx \frac{\Delta\mu_{10}^2 \times \mu_{10}^2}{\sqrt{(\omega_{10}-\omega)^6+\omega_D^6}} - \frac{\mu_{10}^4}{\sqrt{\omega_{10}^2(\omega_{10}-\omega)^4+\omega_D^6}} + \text{cross terms}, \tag{16}$$

where the subscript ''1'' is used to represent the excited state, ''0'' represents the ground state and a damping term, ω_D, is added to allow the use of this equation in fitting the experimental data (see discussion in Ref. 12). The *cross terms* that appear in Eq. (16) approximately cancel out and can be safely ignored.[29] The most appropriate value for ω_D is 250 cm^{-1}, an upper limit to the homogeneous linewidth in bR[34] [see also discussion following Eq. (36) in Ref. 12]. Fortunately, our subsequent calculations are not overly sensitive to assignment of the damping term provided this term is below 1000 cm^{-1}. It was our hope that we could use Eq. (16) to examine the molecular electronic properties responsible for the large second order hyperpolarizability of bacteriorhodopsin. We therefore used weighted nonlinear least-squares procedures to fit Eq. (16) to the Onsager elliptical experimental data. The weighting factors of the data points were assigned to be linearly proportional to the protein concentration. However, as might be anticipated by an examination of Eq. (16), the values of μ_{10} and $\Delta\mu_{10}$ are highly correlated. That is, a unique simultaneous fit of these two variables is not possible. We explore their inter-relationship in Fig. 8, which presents the error contours as a function of the oscillator strength (y axis) and the change in dipole moment (x axis). The minimum error contour is shown with a gray dotted line, and is given by the equation:

$$\Delta\mu_{10}(\text{D}) \approx 0.5515 \times f_{10}^{1.274} + 11.386 \times f_{10}^{-0.4943} - 0.3678. \tag{17}$$

Two-photon studies indicate that there are in fact two allowed low-lying states, the lowest energy $^1B_u^{*+}$-like state ($\lambda_{\max} \approx 568$ nm, $f = 0.8 \pm 0.07$, $\Delta\mu = 13.5 \pm 0.8$ D) and a higher energy $^1A_g^{*-}$-like state ($\lambda_{\max} \approx 488$ nm, $f = 0.3 \pm 0.15$, $\Delta\mu = 9.1 \pm 4.8$ D).[12] These results suggest that in the near-resonant region, the $^1B_u^{*+}$-like state is the dominant contributor to $\gamma(-\omega;0,0,\omega)$. This conclusion follows from considerations of energy, oscillator strength, and dipole moment change, all three of which favor participation of the $^1B_u^{*+}$-like state in enhancing $\gamma(-\omega;0,0,\omega)$. Simulations based on a three state model and the above parameters indicate that the contribution of the $^1B_u^{*+}$-like state relative to the $^1A_g^{*-}$-like state increases from ~ 100 at 676 nm to ~ 325 at 633 nm. This is further evidence that the two-state model is adequate for analyzing the results in this region of the spectrum. The two state model predicts $\Delta\mu_{10} = 12.8$ D and $\omega_{10} = 2.117$ eV (Table IV) assuming $f_{10} = 0.8$ ($\mu_{10} = 9.98$ D).[12] If we include the error range in f_{10} and experimental error in our experimental measurements, the error contour analysis presented in Fig. 8 predicts that the dipole moment difference between the $^1B_u^{*+}$-like π,π^* state and the ground state is 12.8 ± 1.2 D. Our assignment is in excellent agreement with the value determined from Stark measurements (12.4 D)[35] and two-photon spectroscopy (13.5 ± 0.8 D).[12] We anticipate that the close agreement between the present measurement of $\Delta\mu_{10}$ and Ponder's Stark measurement[35] is largely fortuitous given the error bars. Because the two-photon method can explicitly measure $\Delta\mu_{10}$ for the lowest-lying $^1B_u^{*+}$-like state, removing all contributions from other participating states, we anticipate that the two-photon value ($\Delta\mu_{10} = 13.5 \pm 0.8$ D) is the most accurate.

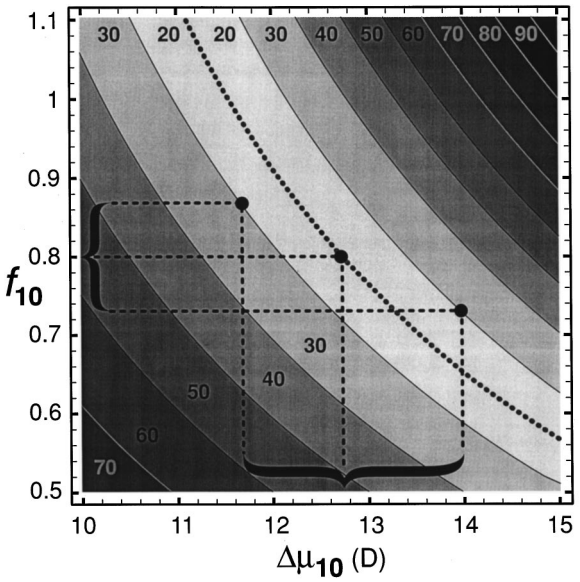

FIG. 8. Error contours for the weighted nonlinear least-squares fit of the Onsager (elliptical) $\gamma(-\omega;0,0,\omega)$ values to the two level model [Eq. (16)]. The individual data points were weighted linearly as a function of the protein concentration. The error contours display the root-mean-square deviation in units of $\gamma(-\omega;0,0,\omega)$ in units of 10^{-32} cm^7 statCoulomb^{-2}. The vertical axis represents the oscillator strength of the $^1B_u^{*+}$-like π,π^* state while the horizontal axis represents the change in dipole moment upon excitation of the same state. Note that $f_{10} = 0.8$ [based on the two-photon analysis (Ref. 12)] dictates a value of $\Delta\mu_{10} = 12.8$ D based on minimization of the error (gray dotted line). The error bar for $\Delta\mu_{10}$ (± 1.2 D) is determined by folding the error range of f_{10} (± 0.07, Ref. 12) onto the expectation value for the experimental error (lowest-error contour lines). The probability that $\Delta\mu_{10}$ is within the range 11.7–14.0 D is 95%.

There is one aspect of Eq. (16) which may not be obvious upon first inspection, but which can have an interesting effect on both the magnitude as well as the frequency depen-

TABLE IV. Second hyperpolarizability $\langle \gamma(-\omega;0,0,\omega)\rangle$ of bacteriorhodopsin as a function of ω and local field factor.[a]

Photon energy Local field	$\omega=1.833$ eV ($\lambda=676$ nm)	$\omega=1.916$ eV ($\lambda=647$ nm)	$\omega=1.959$ eV ($\lambda=633$ nm)
Lorentz (spherical)	8.0 ± 3.7	24 ± 13	76 ± 48
Lorentz (elliptical)	11.2 ± 5.2	33 ± 18	106 ± 67
Onsager (spherical)	7.7 ± 3.6	24 ± 12	71 ± 47
Onsager (elliptical)	10.8 ± 5.1	32 ± 18	103 ± 65
Two state model[b]	15.92	46.06	96.07
AM1[c]	3.06	5.51	7.97
PM3[c]	3.12	5.72	8.38
MNDO[c]	6.16	14.35	25.43

[a] $\langle \gamma(-\omega;0,0,\omega)\rangle$ in units of 10^{-32} cm^7 statCoulomb^{-2}. All values in this table can be converted to SI units ($F^3\,m^4\,C^{-2}$) by multiplying by the conversion factor: 1.238×10^{-25} $F^3\,m^4\,C^{-2}/(cm^7\,statCoulomb^{-2})$. Thus, in SI units, the Onsager (elliptical) $\langle \gamma(-\omega;0,0,\omega)\rangle$ values are 1.34 ± 0.63, 4.0 ± 2.2 and 12.8 ± 8.0 in units of 10^{-56} $F^3\,m^4\,C^{-2}$ at $\omega=1.833$, 1.916, and 1.959, respectively.

[b] $\langle \gamma(-\omega;0,0,\omega)\rangle$ based on Eq. (16) and a weighted nonlinear least-squares fit to the Onsager (elliptical) experimental results and the following parameters: $\Delta\mu_{10}=12.8$ D, $f_{10}=0.8(\mu_{10}=9.98$ D), $\omega_{10}=2.117$ eV, $\omega_D=0.031$ eV(250 cm^{-1}).

[c] Time dependent Hartree–Fock methods based on the AM1, PM3, and MNDO Hamiltonians within MOPAC93 (see the text).

dence of $\gamma(-\omega;0,0,\omega)$. The denominator of the first term decreases in magnitude faster than the denominator of the second term as ω approaches ω_{10}. If the molecule has a low-lying excited singlet state that is both strongly allowed and undergoes a large change in dipole moment upon excitation, the first term will dominate and we will experience type III enhancement (Fig. 9).[36] Symmetric, non-polar molecules with strongly allowed low-lying excited singlet states will yield $\gamma(-\omega;0,0,\omega)$ values that are enhanced primarily via the second term. This type of enhancement is called

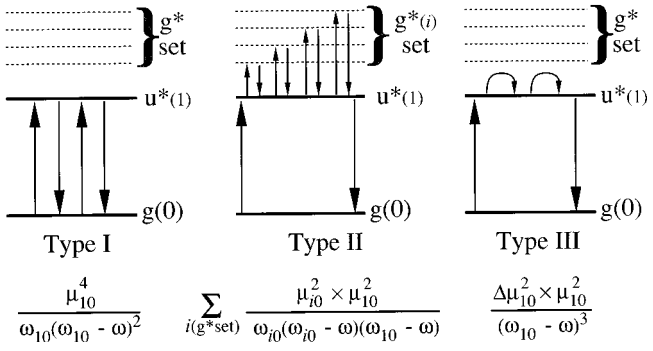

FIG. 9. Schematic diagrams showing the molecular electronic origins of the type I, type II, and type III second-order hyperpolarizability enhancement processes. The symbol $g(0)$ denotes the ground state of the all-*trans* protonated Schiff base chromophore and $u^*(1)$ denotes the lowest-lying, strongly-allowed $^1B_u^{*+}$-like π,π^* state. The $g^*(i)$ set of states includes all the higher energy $^1A_g^*$-like π,π^* states with non-negligible transition moments with the lowest-lying $^1B_u^{*+}$-like state. Arrows between different states correspond to electronic transition moments. Arrows that return to the same state indicate electron reorganization resulting in dipole moment changes of that state relative to the ground state. The principal terms responsible for the enhancement based on the two-state (types I and III) and expanded multistate (type II) approximations are shown below the relevant diagrams.

''type I'' enhancement (Fig. 9).[36] Clearly, the second hyperpolarizability of bacteriorhodopsin is dominated by type III enhancement, because $\Delta\mu_{10}>\mu_{10}$.[15,20] If the two-state approximation were rigorously accurate, type III enhancement could be verified experimentally by observing a sign change in $\gamma(-\omega;0,0,\omega)$ at the frequency

$$\omega_Q=\omega_{10}[1+(\Delta\mu_{10}/\mu_{10})^2]. \tag{18}$$

However, in the present case, this frequency is in the ultraviolet ($\sim$5.6 eV, $\sim$220 nm), and other electronic states would dominate $\gamma(-\omega;0,0,\omega)$.

D. Comparison with theory

Time-dependent Hartree–Fock molecular orbital theory represents one of the more accurate methods available for calculating molecular hyperpolarizabilities.[37] Kurtz and Korambath have implemented versatile iterative procedures for calculating α, β, and γ based on time-dependent methods within the MOPAC93 package.[38,39] We used these methods to calculate $\gamma(-\omega;0,0,\omega)$ as a function of energy using for comparative purposes the AM1, PM3, and MNDO Hamiltonians. The iterative procedures are highly computationally intensive, particularly under resonance conditions. Despite the use of semiempirical Hamiltonians, we had to limit the calculation to the all-*trans* protonated Schiff base chromophore to achieve convergence at energies above 1.95 eV. The results are presented in the bottom three rows of Table IV.

The MNDO calculations do a relatively good job of reproducing the observed second-order hyperpolarizability considering the level of approximation and the fact that we are limiting the calculation to the chromophore. The fact that all three semiempirical parameterizations underestimate $\gamma(-\omega;0,0,\omega)$ may also be due to the inherent tendency of all three methods to underestimate dipole moment changes and inaccurately represent transition energies into the low-lying excited singlet states.[25,40] We note that all calculations were carried out using the standard parameterization optimized for the ground state. Nevertheless, we consider the results from the MNDO calculations to be worth noting and suggest that this Hamiltonian is the best choice for calculating the hyperpolarizabilities of molecules using time-dependent Hartree–Fock methods with MOPAC.

IV. COMMENTS AND CONCLUSIONS

We have examined the quadratic electrooptic effects (dc or low frequency Kerr effect) of bacteriorhodopsin dispersed in dried gelatin thin films. Data were collected at three wavelengths: 632.8 nm (He–Ne), 647.1 nm (Kr ion) and 676.4 nm (Kr ion). These wavelengths correspond to the near absorption edge region of the ground state of the bacteriorhodopsin (Fig. 1). The films show relatively large quadratic electrooptic effects compared to other molecular dispersed systems. The purple membrane is fixed within the polymerized gelatin matrix, and we show that the electronic contribution to γ dominates over possible orientational contributions. At 676 nm, the quadratic electrooptic coefficient $s_{1133}(-\omega;0,0,\omega)$ is 6.7×10^{-20} m^2/V^2 and the third order nonlinear susceptibility

$\chi^{(3)}_{1133}(-\omega;0,0,\omega)$ is 7.0×10^{-13} cm^4 statCoulomb^{-2}, with both values obtained for a protein concentration of 6.9×10^{18} cm^{-3}. The value of $s_{1133}(-\omega;0,0,\omega)$ varies linearly with protein concentration indicating that the protein, and only the protein, is responsible for the observed hyperpolarizability. The orientationally averaged second molecular hyperpolarizability $\langle\gamma(-\omega;0,0,\omega)\rangle$ determined from the quadratic electro-optic coefficients at 676 nm assuming an Onsager ellipsoidal local field factor is $(10.8\pm5.1)\times10^{-32}$ cm^7 statcoulomb^{-2}. The value of $\langle\gamma(-\omega;0,0,\omega)\rangle$ increases tenfold to $(103\pm65)\times10^{-32}$ cm^7 statcoulomb^{-2}, when the probe wavelength is decreased to 633 nm.

Quadratic electrooptic effects measured at 633 nm are enhanced at high incident light intensities. We suggest that this enhancement is due to the stationary state accumulation of the **O** intermediate of bacteriorhodopsin, which strongly absorbs the irradiation at 633 nm. We were able to compensate for this source of error by extrapolating the data back to low photon densities.

The $\gamma(-\omega;0,0,\omega)$ values as a function of ω were fit to a two-state model of the form

$$\gamma_{10}(-\omega;0,0,\omega)\approx\frac{\Delta\mu_{10}^2\times\mu_{10}^2}{\sqrt{(\omega_{10}-\omega)^6+\omega_D^6}}-\frac{\mu_{10}^4}{\sqrt{\omega_{10}^2(\omega_{10}-\omega)^4+\omega_D^6}}+\text{cross terms},$$

where $\Delta\mu_{10}$ is the change in dipole moment, μ_{10} is the transition moment, and ω_{10} is the transition energy of the lowest-lying allowed $^1B_u^{*+}$-like π,π^* state. Our weighted nonlinear least squares fit indicates that $\gamma(-\omega;0,0,\omega)$ is strongly enhanced via type III processes. That is, the magnitude of $\gamma(-\omega;0,0,\omega)$ is dominated by the first term. We calculate that the dipole moment difference between the $^1B_u^{*+}$-like π,π^* state and the ground state is 12.8 ± 1.2 D, in good agreement with the value determined from Stark measurements (12.4 D) and two-photon spectroscopy (13.5 ± 0.8 D).

Time-dependent Hartree–Fock methods based on the MNDO Hamiltonian yield reasonable agreement with experiment, underestimating $\gamma(-\omega;0,0,\omega)$ by factors of only 2–4, with the error increasing as the frequency approaches resonance. The AM1 and PM3 calculations were much less reliable, and thus we recommend use of the MNDO Hamiltonian for calculating hyperpolarizabilities within the MOPAC package.

ACKNOWLEDGMENTS

This work was supported in part by the National Institutes of Health (GM-34548). Specialized instrumentation was funded by the W. M. Keck Foundation. The authors thank Dr. Charles Martin and Igor Barani for their help with the theoretical calculations, and Bryan Vought and Constance Birge for help in preparing purified bacteriorhodopsin. We thank Jeff Stuart, Jack Tallent and Eric Tan for many helpful discussions.

APPENDIX A: THE ELLIPSOIDAL LOCAL FIELD FACTORS

The local field factor is defined as a ratio of an amplitude of the internal field $\mathbf{E}_i$ to that of the external field $\mathbf{E}_0$. The local field factor for a dipole placed in an ellipsoidal cavity was derived based on the theory of electric polarization described by Onsager[18] and Böttcher.[41]

We have two major effects to be considered to obtain an approximate field strength interacting with a dipole inside of the ellipsoidal cavity,[42] namely, (1) The cavity field: $\mathbf{E}_c$, (2) Reaction field: $\mathbf{R}$. The internal field $\mathbf{E}_i$ should be a sum of the cavity field and the reaction field, that is,

$$E_i=E_c+R. \tag{A1}$$

Additional field that arises from orientation of permanent dipoles and is called the directional field E_d should be considered if one works with liquid or gas phase. However, purple membrane is fixed in the gelatin matrix by the cross linked structure of the gelatin with hydrogen bonds, and the purple membrane is considered to be randomly oriented even under the external electric field. The effect from the directional field is therefore ignored here.

The cavity field for the ellipsoidal cavity is given by[43]

$$(\mathbf{E}_c)_\alpha=\frac{\epsilon_2}{\epsilon_2+(1-\epsilon_2)A_\alpha}E_0,\qquad \alpha\in\{a,b,c\} \tag{A2}$$

ϵ_2 is dielectric constant of the matrix and A_α is an ellipsoidal shape factor given by

$$\left.\begin{aligned}A_\alpha&=\frac{abc}{2}\int_0^\infty\frac{ds}{(s+\alpha^2)R_s}\\R_s&=\sqrt{(s+a^2)(s+b^2)(s+c^2)}\\\alpha&\in\{a,b,c\}\end{aligned}\right\}, \tag{A3}$$

where a, b, and c are semimajor axes of the ellipsoidal cavity.

Meanwhile, the linear polarizability α_a, the reaction field factor f_a and the reaction field R_a in the a direction are given as

$$\left.\begin{aligned}\alpha_a&=\frac{(\epsilon_1-1)}{3\{1+(\epsilon_1-1)A_a\}}abc\\f_a&=\frac{3}{abc}\frac{A_a(1-A_a)(\epsilon_2-1)}{\epsilon_2+(1-\epsilon_2)A_a}\\R_a&=\frac{f_a\alpha_a}{1-f_a\alpha_a}E_c\end{aligned}\right\}. \tag{A4}$$

Assuming the direction of the external field E_0 is along the semimajor axis of the ellipsoid, a, substitution of (A4) into (A1) yields

$$E_i=\frac{1}{1-f_a\alpha_a}E_c=\frac{1}{1-f_a\alpha_a}\frac{\epsilon_2}{\epsilon_2+(1-\epsilon_2)A_a}E_0=\frac{\epsilon_2\{1+(\epsilon_1-1)A_a\}}{\epsilon_2+(\epsilon_1-\epsilon_2)A_a}E_0. \tag{A5}$$

From (A5), the local field factor at a static field for the ellipsoidal cavity is obtained as

$$f^{(0)}_{\text{ellipse}}=\frac{\epsilon_2(0)\{1+(\epsilon_1(\omega)-1)A_a\}}{\epsilon_2(0)+(\epsilon_1(\omega)-\epsilon_2(0))A_a} \tag{A6}$$

by letting ϵ_1 be a permittivity at an optical frequency $\epsilon_1(\omega)$ and ϵ_2 a permittivity at static field $\epsilon_2(0)$. For a field at an optical frequency, by assigning ϵ_1 and ϵ_2 to represent permittivities at optical frequencies $\epsilon_1(\omega)$ and $\epsilon_2(\omega)$, respectively, we obtain

$$f^{(\omega)}_{\text{ellipse}}=\frac{\epsilon_2(\omega)\{1+(\epsilon_1(\omega)-1)A_a\}}{\epsilon_2(\omega)+(\epsilon_1(\omega)-\epsilon_2(\omega))A_a}. \tag{A7}$$

For a spherical cavity, $A_a=1/3$. In such a case (A6) is reduced to

$$f^{(0)}_{\text{spherical}}=\frac{\epsilon_2(0)(\epsilon_1(\omega)+2)}{2\epsilon_2(0)+\epsilon_1(\omega)} \tag{A8}$$

which is identical to the Onsager's local field factor for a spherical cavity. Similarly for the ellipsoidal local field factor at optical frequency, a spherical local field factor at an optical frequency is obtained from (A7)

$$f^{(\omega)}_{\text{sperical}}=\frac{\epsilon_2(\omega)(\epsilon_1(\omega)+2)}{2\epsilon_2(\omega)+\epsilon_1(\omega)}. \tag{A9}$$

In a more simple physical picture than the Onsager's model, where the reaction field is not taken into account, the local field can be written as sum of an external field and a polarization field inside an ellipsoidal cavity or a spherical cavity. The extent to which the polarization P_2 affects the internal field is given by the depolarizing tensor $\mathbf{L}$

$$\mathbf{E}_i=\mathbf{E}_0+4\pi\mathbf{L}\cdot\mathbf{P}_2. \tag{A10}$$

Substituting $P_2=(\epsilon_2-1)E_0/4\pi$, where ϵ_2 is a permittivity of the dielectric, into (A10) and rearrangement yields

$$\mathbf{E}_i=[\mathbf{I}+(\epsilon_2-1)\mathbf{L}]\cdot\mathbf{E}_0. \tag{A11}$$

The diagonal components of $\mathbf{L}$, L_α, are equal to A_α when the shapes of the molecule and the cavity are ellipsoidal. Consequently, the internal field is given by

$$\mathbf{E}_i=[\mathbf{I}+(\epsilon_2-1)\mathbf{A}]\cdot\mathbf{E}_0. \tag{A12}$$

Because $\mathbf{A}$ is a diagonal tensor,

$$E_i=[1+(\epsilon_2-1)A_\alpha]E_0,\qquad \alpha\in\{a,b,c\}. \tag{A13}$$

Assuming the direction of the external field E_0 is along the semimajor axis of the ellipsoid, a, the Lorentz-type local field factor for the ellipsoidal cavity is thereby defined as

$$f^{(\omega)}_{\text{ellipse}}=1+(\epsilon_2(\omega)-1)A_a. \tag{A14}$$

For a spherical cavity, $A_a=1/3$. Then (A14) is reduced to

$$f^{(\omega)}_{\text{sphere}}=\frac{\epsilon_2(\omega)+2}{3} \tag{A15}$$

$f^{(0)}_{\text{ellipse or sphere}}$ are also defined for the Lorentz-type local field factors similarly to those defined for the Onsager type local field factors

$$f^{(0)}_{\text{ellipse}}=1+(\epsilon_2(0)-1)A_a, \tag{A16}$$

$$f^{(0)}_{\text{sphere}}=\frac{\epsilon_2(0)+2}{3}. \tag{A17}$$

APPENDIX B: RELATION BETWEEN $\chi^{(3)}(-\omega;0,0,\omega)$ AND $\gamma(-\omega;0,0,\omega)$

A third order macroscopic polarization at an optical frequency ω is given by

$$P^{(\omega)}_i=\chi^{(3)}_{ijkl}E^{(0)}_j E^{(0)}_k E^{(\omega)}_l \tag{B1}$$

while a microscopic polarizability for each molecule at an optical frequency ω is given by

$$p^{(\omega)}_{i'}=\gamma_{i'j'k'l'}(-\omega;0,0,\omega)(E^{(0)}_{\text{local}})_{j'}(E^{(0)}_{\text{local}})_{k'}(E^{(\omega)}_{\text{local}})_{l'}. \tag{B2}$$

Here, $(i,j,k,l,\ldots)$ denotes indices for film coordinates while $(i',j',k',l',\ldots)$ denotes indices for molecular coordinates for each molecule. This quantity corresponds to an induced dipole moment of a molecule. $\mathbf{E}_{\text{local}}$ is a local field corrected electric field and related to external field as

$$(E^{(0)}_{s,\ \text{local}})_{i'}=(f^{(0)}_{s,\text{ellipse}})_{i'j'}(E^{(0)}_{j'}). \tag{B3}$$

The third order polarization can be related to the microscopic polarizability with the local field factors

$$P^{(\omega)}_i=\sum_{s=1}^{N}R^s_{ii'}(f^{(\omega)}_{s,\text{ellipse}})_{i'j'}(p^{(\omega)}_s)_{j'}. \tag{B4}$$

Similarly, relation between the macroscopic susceptibility $\chi^{(3)}$ and the microscopic susceptibility γ is

$$\chi^{(3)}_{ijkl}(-\omega;0,0,\omega)=N\langle R_{im'}R_{jn'}R_{ko'}R_{lp'}f^{(\omega)}_{m'i'}\times\gamma_{i'j'k'l'}(-\omega;0,0,\omega)f^{(0)}_{j'n'}f^{(0)}_{k'o'}f^{(\omega)}_{l'p'}\rangle. \tag{B5}$$

$\mathbf{R}^s_{ii'}$ is a tensor that converts a molecular coordinate of sth molecule i' to a coordinate i fixed in the film. For simplicity, we will calculate an orientational average of the microscopic susceptibility γ and try to relate it to the macroscopic susceptibility $\chi^{(3)}$.

The orientational average of γ can be obtained by examining the symmetry of permutations of the applied fields for the expression of $\gamma(-\omega;0,0,\omega)$ given by Orr and Ward[44] and by taking known nonzero components of γ for the point group of the molecule (C_1 in this case) into account. By neglecting the damping terms, their expression can be reduced in the near resonance or resonance region to

$$\begin{aligned}&\gamma_{i'j'k'l'}(-\omega_\sigma;\omega_1,\omega_2,\omega_3)\\&=4K(-\omega_\sigma;\omega_1,\omega_2,\omega_3)(-\hbar)^3I_{-\sigma,1,2,3}\\&\times\Bigg[\sum_{lmn\neq g}\frac{\langle g|\mu_{i'}|l\rangle\langle l|\mu_{l'}|m\rangle\langle m|\mu_{k'}|n\rangle\langle n|\mu_{j'}|g\rangle}{(\omega_{lg}-\omega_\sigma)(\omega_{mg}-\omega_1-\omega_2)(\omega_{ng}-\omega_1)}\\&-\sum_{lmn\neq g}\frac{\langle g|\mu_{i'}|m\rangle\langle m|\mu_{l'}|g\rangle\langle g|\mu_{k'}|n\rangle\langle n|\mu_{j'}|g\rangle}{(\omega_{mg}-\omega_\sigma)(\omega_{ng}-\omega_1)(\omega_{ng}+\omega_2)}\Bigg],\end{aligned} \tag{B6}$$

where I denotes the average of all terms generated by permuting $-\omega_\sigma$, ω_1, ω_2, and ω_3 and K is a numerical factor with labels in (B6) and whose value depends on the presence of zero frequencies and repeated frequency in the set ω_σ, ω_1, ω_2, and ω_3. $\mu_{i'}$ is a ground state dipole moment of the chromophore along i' direction in the molecular coordinate. $|n\rangle$ and $|g\rangle$ denote state vectors for a nth state and a ground state of the chromophore, respectively.

By noting that: (1) two of the four frequencies in Eq. (B6) are equal, i.e., either 0 or ω, (2) Eq. (B6) allows exchange between the indices i' and j' and between k' and l' (3) all components are nonzero for C_1 symmetry, one obtains the orientationally averaged value of γ for a tensor component measured in the experiment with respect to the film coordinates as[45,46]

$$\begin{aligned}
&\langle \gamma_{i'j'k'l'}(-\omega;0,0,\omega)\rangle_{ijkl} \\
&\quad = \tfrac{1}{5}(\gamma_{xxxx}+\gamma_{yyyy}+\gamma_{zzzz})+\tfrac{1}{15}(\gamma_{xxyy}+\gamma_{xyxy}+\gamma_{xyyx} \\
&\qquad +\gamma_{yyxx}+\gamma_{yxyx}+\gamma_{yxxy})+\tfrac{1}{15}(\gamma_{xxzz}+\gamma_{xzxz}+\gamma_{xzzx} \\
&\qquad +\gamma_{zzxx}+\gamma_{zxzx}+\gamma_{zxxz})+\tfrac{1}{15}(\gamma_{yyzz}+\gamma_{yzyz}+\gamma_{yzzy} \\
&\qquad +\gamma_{zzyy}+\gamma_{zyzy}+\gamma_{zyyz}) \\
&\quad = \tfrac{1}{5}(\gamma_{xxxx}+\gamma_{yyyy}+\gamma_{zzzz})+\tfrac{1}{15}(4\gamma_{xxyy}+\gamma_{xyyx}+\gamma_{yxxy}) \\
&\qquad +\tfrac{1}{15}(4\gamma_{xxzz}+\gamma_{xzzx}+\gamma_{zxxz})+\tfrac{1}{15}(4\gamma_{yyzz}+\gamma_{yzzy} \\
&\qquad +\gamma_{zyyz}) \qquad \text{(B7)}
\end{aligned}$$

with

$$\gamma_{i'i'j'j'}=\gamma_{j'j'i'i'}=\gamma_{i'j'i'j'}=\gamma_{j'i'j'i'}\neq\gamma_{i'j'j'i'}\neq\gamma_{j'i'i'j'}, \quad i'\neq j'\in\{x,y,z\}. \qquad \text{(B8)}$$

Using (B7), (B5) can be rewritten for isotropic medium as

$$\begin{aligned}
&\chi^{(3)}_{ijkl}(-\omega;0,0,\omega) \\
&\quad = N f^{(0)}_{\text{ellipse}}\, f^{(0)}_{\text{ellipse}}\, f^{(\omega)}_{\text{ellipse}}\, f^{(\omega)}_{\text{ellipse}}\langle \gamma(-\omega;0,0,\omega)\rangle_{ijkl}. \qquad \text{(B9)}
\end{aligned}$$

$\langle\ \rangle_{ijkl}$ here denotes an average value over the molecular coordinates x,y,z and experimentally measured value as a tensor component specified with the indices for the film coordinate i,j,k,l. Because the local field factors are constants at specific frequency, the linear relationship between $\chi^{(3)}$ and γ found in (B9) is assured by the observation of a linear relationship between s_{1133} and concentration (Fig. 5).

[1] D. Oesterhelt and W. Stoeckenius, Nature (London), New Biol. **233**, 149 (1971).
[2] R. R. Birge, Biochim. Biophys. Acta **1016**, 293 (1990).
[3] R. A. Mathies, S. W. Lin, J. B. Ames, and W. T. Pollard, Annu. Rev. Biophys. Biophys. Chem. **20**, 491 (1991).
[4] M. A. El-Sayed, Acc. Chem. Res. **25**, 279 (1992).
[5] T. G. Ebrey, in *Thermodynamics of Membrane Receptors and Channels*, edited by M. B. Jackson (CRC Press, Boca Raton, 1993), pp. 353–387.
[6] H. Tributsch and R. A. Bogomolni, Chem. Phys. Lett. **227**, 74 (1994).
[7] R. R. Birge, Nature (London) **371**, 659 (1994).
[8] J. K. Lanyi, Nature (London) **375**, 461 (1995).
[9] N. Grigorieff, T. A. Ceska, K. H. Downing, J. M. Baldwin, and R. Henderson, J. Mol. Biol. **259**, 393 (1996).
[10] J. A. Stuart and R. R. Birge, in *Biomembranes*, Vol. 2A, edited by A. G. Lee (JAI, London, 1996), pp. 33–140.
[11] G. Haran, K. Wynne, A. Xie, Q. He, M. Chance, and R. M. Hochstrasse, Chem. Phys. Lett. **261**, 389 (1996).
[12] R. R. Birge and C. F. Zhang, J. Chem. Phys. **92**, 7178 (1990).
[13] R. R. Birge, P. A. Fleitz, A. F. Lawrence, M. A. Masthay, and C. F. Zhang, Mol. Cryst. Liq. Cryst. **180**, 107 (1990).
[14] R. R. Birge, Annu. Rev. Phys. Chem. **41**, 683 (1990).
[15] R. R. Birge, M. B. Masthay, J. A. Stuart, J. R. Tallent, and C. F. Zhang, Proc. SPIE **1432**, 129 (1991).
[16] R. R. Birge, R. B. Gross, M. B. Masthay, J. A. Stuart, J. R. Tallent, and C. F. Zhang, Mol. Cryst. Liq. Cryst. Sci. Technol. Sec. B. Nonlinear Optics **3**, 133 (1992).
[17] Z. Chen, A. Lewis, H. Takei, and I. Nabenzahl, Appl. Opt. **30**, 5188 (1991).
[18] J. Y. Huang, A. Lewis, and T. Rasing, J. Phys. Chem. **92**, 1756 (1988).
[19] J. Y. Huang, Z. Chen, and A. Lewis, J. Phys. Chem. **93**, 3314 (1989).
[20] R. R. Birge, P. A. Fleitz, A. F. Lawrence, M. A. Masthay, and C. F. Zhang, Mol. Cryst. Liq. Cryst. **189**, 107 (1990).
[21] J. S. Schildkraut, Appl. Phys. Lett. **61**, 2839 (1990).
[22] Z. Z. Ho, R. T. Chen, and R. Shih, Appl. Phys. Lett. **61**, 4 (1992).
[23] A. Yariv, *Quantum Electronics*, 3rd ed. (Wiley, New York, 1988).
[24] C. C. Teng and H. T. Man, Appl. Phys. Lett. **56**, 1734 (1990).
[25] J. A. Stuart, B. W. Vought, C. F. Zhang, and R. R. Birge, Biospectroscopy **1**, 9 (1995).
[26] J. R. Tallent, J. R. Birge, C. F. Zhang, E. Wenderholm, and R. R. Birge, Photochem. Photobiol. **56**, 935 (1992).
[27] Q. W. Song, C. Y. Ku, R. B. Gross, R. R. Birge, and R. Michalak, J. Opt. Soc. Am. B **12**, 797 (1995).
[28] A. K. Dioumaev and M. S. Braiman, J. Am. Chem. Soc. **117**, 10572 (1995).
[29] M. G. Kuzyk, J. E. Sohn, and C. W. Dirk, J. Opt. Soc. Am. B **7**, 842 (1990).
[30] M. Ponder and R. Mathies, J. Phys. Chem. **87**, 5090 (1983).
[31] A. B. Myers and R. R. Birge, J. Am. Chem. Soc. **103**, 1881 (1981).
[32] E. Bradbury and C. Martin, Proc. R. Soc. London A **214**, 183 (1952).
[33] A. B. Myers and R. R. Birge, J. Chem. Phys. **74**, 3514 (1981).
[34] A. B. Myers, R. A. Harris, and R. A. Mathies, J. Chem. Phys. **79**, 603 (1983).
[35] M. C. Ponder, Ph.D., University of California, Berkeley, 1983.
[36] A. F. Garito, J. R. Helfin, K. Y. Wong, and O. Zamani-Khamiri, in *Organic Materials for Non-linear Optics*, edited by R. A. Hann and D. Bloor (Royal Society of Chemistry, London, 1989), pp. 16–27.
[37] M. Dupuis and S. Kama, J. Comput. Chem. **12**, 487 (1991).
[38] J. J. P. Stewart, MOPAC93, (Fujitsu Ltd., 1993).
[39] J. J. P. Stewart, MOPAC93 Manual (1993).
[40] C. H. Martin and R. R. Birge, J. Phys. Chem. **102**, 852 (1998).
[41] C. J. F. Böttcher, O. C. van Bell, P. Bordewijk, and A. Rip, *Theory of Electric Polarization*, Vol. I, Dielectrics in Static Fields (Elsevier Scientific, New York, 1973).
[42] L. Onsager, J. Am. Chem. Soc. **58**, 1486 (1936).
[43] J. A. Stratton, *Electromagnetic Theory* (McGraw-Hill, New York, 1941).
[44] B. J. Orr and J. F. Ward, Mol. Phys. **20**, 513 (1971).
[45] B. M. Pierce, J. Chem. Phys. **91**, 791 (1989).
[46] A. D. Buckingham and M. J. Stephen, Trans. Faraday Soc. **53**, 884 (1957).